Angewandte Chemie
Eine Zeitschrift der Gesellschaft Deutscher Chemiker

Supporting Information

Highly Durable Inverted Inorganic Perovskite/Organic Tandem Solar Cells Enabled by Multifunctional Additives

Y. Li, Y. Yan, Y. Fu, W. Jiang, M. Liu, M. Chen, X. Huang, G. Lu, X. Lu, J. Yin, S. Wu*, A. K.-Y. Jen**

Supporting Information

Highly Durable Inverted Inorganic Perovskite/Organic Tandem Solar Cells Enabled by Multifunctional Additives

Yanxun Li[1,2,#], Yichao Yan[1,2,9,#], Yuang Fu[8], Wenlin Jiang[1,2], Ming Liu[1,2], Mingqian Chen[1,2], Xiaofeng Huang[2,3], Guanghao Lu[7], Xinhui Lu[8], Jun Yin[6,*], Shengfan Wu[1,2,*], Alex K.-Y. Jen[1,2,3,4,5,*]

[1] Department of Materials Science & Engineering, City University of Hong Kong, Kowloon, Hong Kong, 999077, China

[2] Hong Kong Institute for Clean Energy, City University of Hong Kong, Kowloon, Hong Kong, 999077, China

[3] Department of Chemistry, City University of Hong Kong, Kowloon, Hong Kong, 999077, China

[4] Department of Materials Science & Engineering, University of Washington, Seattle, Washington, 98195, United States

[5] State Key Laboratory of Marine Pollution, City University of Hong Kong, Kowloon, Hong Kong, 999077, China

[6] Department of Applied Physics, The Hong Kong Polytechnic University, Kowloon, Hong Kong, 999077, China

[7] Frontier Institute of Science and Technology, Xi'an Jiaotong University, Xi'an, 710054, China

[8] Department of Physics, The Chinese University of Hong Kong, New Territories, Hong Kong, 999077, China

[9] School of Sustainable Energy and Resources, Nanjing University, Suzhou, Jiangsu, 215163 P. R. China

[#] These authors contributed equally for this work.

*Corresponding authors, e-mail: alexjen@cityu.edu.hk; shengfwu2@cityu.edu.hk; jun.yin@polyu.edu.hk

Methods

Materials. The reagents and starting materials in the synthesis of AQS-based additives were commercially available and used without any further purification. Caesium iodide (CsI) was purchased from Dysol. Lead iodide (PbI_2, purity of 99.999%), lead bromide ($PbBr_2$, purity of 99.9%) and DIO was purchased from TCI. Lead chloride ($PbCl_2$), DMAI CF3-PEAI, fullerene (C60) and BCP (purity of 99.9%) were purchased from Xi'an Polymer Light Technology Corporation. DMF (99.99%), DMSO (99.50%) and IPA (99.50%) were purchased from J&K. Chloroform (CF) and methanol (MA) were purchased from Sigma-Aldrich. PM6 and BTP-eC9 were purchased from Solarmer Materials. PCBM was purchased from American Dye Source, Inc.

Solution preparation. 10 mg NiO_x nanoparticle was sonically dispersed into 1 mL deionized water. The CbzNaph was dissolved in IPA with a concentration of 1 mg/mL. To prepare the control inorganic perovskite precursor, 0.95M CsI:$PbBr_2$:PbI_2:$PbCl_2$ (molar ratio=1:0.6:0.4:0.1) were disolved in a mixed solution of DMF:DMSO (vt:vt=1:1.4) and 0.86M DMAI was added to regulate the annealing temperature. Target precursors were added 0.1% molar ratio AQS-FPMA and AQS:FPEA, respectively. The CF_3-PEAI was prepared with a concentration of 1 mg/mL in IPA. The PM6:BTP-eC9:PCBM (wt:wt:wt = 1:1.1:0.1) was disolved in CF with a donor concentration of 7 mg/mL and 0.5% vt DIO was added in the blend as the additive. The PNDIT-F3N solution was prepared by disolving 0.5 mg PNDIT-F3N in 1 mL methanol and 5 uL acetic acid.

Inorganic perovskite solar cells fabrication. The single-junction inorganic perovskite solar cells (i-PSCs) were fabricated based on a structure including ITO/NiO_x/CbzNaph/i-PVK/C_{60}/BCP/Ag. First, the ITO-coated substrates were cleaned with distilled water, acetone, and isopropanol (IPA) in an ultrasonic bath followed by ultraviolet-ozone treatment for 15 minutes. Before device fabrication, the substrates were placed in a 65 ^oC oven for overnight to dry. Second, substrates were plasma treated for 15 minutes for further device fabrication. Third, the NiO_x

nanoparticle was spin-coated on the ITO substrate and then followed to be annealed at 120 ^{o}C for 20 minutes. Four, the CbzNaph solution was spin-coated on the substrate and annealed at 100 ^{o}C for 10 minutes. Then, 50 uL isopropanol (IPA) was spun onto the substrate to remove unbound molecules and further annealed at 100 ^{o}C for 5 minutes to get the self-assembled monolayer. Five, 60 uL i-PVK precursor solution was spin-coated on the substrate at optimized speed and then annealed at 170 ^{o}C for 20 minutes in an air glovebox. Six, the CF_3-PEAI solution was spin-coated on the perovskite to passivate surface. Finally, substrates were transferred in a vacuum evaporation chamber to deposite 25 nm C_{60}, 6 nm BCP and 100 nm Ag in sequence to get final devices.

Single-junction organic solar cells fabrication. The single-junction organic solar cells (OSCs) were fabricated with a structure of ITO/MoO_x/PM6:BTP-eC9:PCBM/PNDIT-F3N/Ag. The clean ITO substrates were plasma treated for 15 minutes. Then they were transferred to a vacuum evaporation chamber to deposit 10 nm MoOx. Next, the PM6:BTP-eC9:PCBM blend was spin-coated on the MoO_x with a film thickness of 110 nm. It was then annealed at 90 ^{o}C for 5 minutes to remove solvent. Further, the PNDIT-F3N was spin-coated on the PM6:BTP-eC9:PCBM as the electron transporting layer. Finally, 100 nm Ag was deposited as the electrode by the vacuum evaporation system.

Tandem solar cells fabrication. The tandem solar cells were fabricated with a structure of ITO/NiO_x/CbzNaph/i-PVK/C_{60}/SnO_x/Au/MoO_x/PM6:BTP-eC9:PCBM/PNDIT-F3N/Ag. The processings to deposite the NiO_x, SAM, i-PVK, and C_{60} layers were same as that of single-junction i-PSCs. The SnO_x of 20 nm was deposited on the C60 film by the ALD method. After the deposition of SnO_x, the coated substrates were transferred in a vacuum evaporation chamber to deposit 0.5 nm Au and 10 nm MoO_x in turn. Then, the OSC subcell was fabricated using the process mentioned above.

Measurements and characterizations. The ^{1}H NMR and ^{13}C NMR spectra were measured on Bruker AVANCE III 300MHz and 400MHz spectrometers. The XRD

patterns for powder analysis are measured by an X-ray diffraction (XRD) using a Bruker D2 Phaser with Cu Kα radiation. The dynamic light scattering (DLS) was performed by a daynamic light scattering particle size Analyzer (Malven Zetasizer Nano ZS) at 25 °C with a monochromatic coherent He–Ne laser (640 nm) as the light source. An avalanche photodiode detector that detected the scattered light at an angle of 173°. The scanning electron microscopy (SEM, Philips XL30 FEG) was performed to obtain the top-viewing morphology of perovskite films. The XPS and UPS sepctra were studied by a VG ESCALAB 220i-XL surface analysis system equipped with a monochromatic Al-Kα X-ray gun (hv = 1486.6 eV) and a He discharge lamp (hv = 21.22 eV). The PL sepctra and TRPL were performed by the Edinburgh Instruments FLS1000 System with a 480-nm pulsed excitation laser. *J-V* characteristics were examined by using a Keithley 2400 SourceMeter under AM1.5G sunlight (calibrated by a certified silicon solar cell with a KG-2 filter) from a solar simulator (SS-F5, EnliTech) in a N_2-filled glovebox at 25 ^oC. The EQE curves were obtained by using the QE-R EnliTech EQE system. Dynamic MPPT was examined on an in-situ stability measurement system (CRYSCO, Guangzhou) under the LED lamp with an intensity equaling 1 sun. The chamber of MPPT was placed in the N_2-filled glovebox. Contact angle was measured with a DataPhysics contact angle tester and the water drop volume was set as 2 μL. The Nyquist plots of electrochemical impedance spectra (EIS) were scanned from 10^6 to 50 Hz with a disturbance AC signal of 20 mV in dark condition by utilizing a CHI760E. The temperature-dependent thermal admittance spectrum (TAS) was performed in a vacuum-chamber testing platform with EIS tests performed every 10 K at the temeperatures ranging from 250 K to 330 K. These EIS were scanned from 10^6 to 50 Hz with a disturbance AC signal of 20 mV in dark condition.

In-situ Characterizations. The in-situ light absorption spectra, fluorescence spectra and light scattering spectra were performed on a multi-spectrometer (DU-200, Shaanxi Puguang Weishi Co. Ltd.). The LED light source is vertically irradiated on the sample through the optical fiber, and the transmission spectrum of 186-1026nm is

detected by the spectrometer. The spectral resolution reaches 0.01nm and the time resolution reaches 1ms. The nucleation and crystallization process of the polymer and small molecules are analyzed by the spectral data, and the morphological characteristics of the film are detected and revealed in real time. In-situ GIWAXS experiments for the perovskite thermal annealing process were conducted at TLS 23A small- and wide-angle X-ray scattering (SWAXS) beamline at the National Synchrotron Radiation Research Center (NSRRC), Hsinchu, Taiwan. The X-ray wavelength was 1.240 Å (10 keV), and the scattering signals were collected by a C9728DK area detector. The sample-to-detector distance was ≈196 mm, calibrated with a lanthanum hexaboride (LaB_6) sample. The sample was placed on a hot plate stabilised at 170 ℃ before measurements started. The serial measurements were performed at an incident angle of 2° for 600 s. The exposure time per frame was 1.9 s, followed by a 0.1 s interval, giving a total of 300 frames.

Density Functional Theory (DFT) Calculation. The DFT calculations were performed using the projector-augmented wave (PAW) method as implemented in the Vienna Ab initio Simulation Package (VASP) code. The generalized gradient approximation (GGA) together with the Perdew-Burke-Ernzerhof (PBE) exchange-correlation functional was used. The van der Waals (vdW) interactions were also included in the calculations using the zero damping DFT-D3 method of Grimme. A uniform grid of 6×6×2 *k*-mesh in the Brillouin zone was employed to optimize crystal structures of DMSO-PbI_2 and AQS-DMSO-PbI_2, and 1×1×1 *k*-mesh for the cluster structures of DMSO-PbI_2 and AQS-PbI_2. The energy cutoff of the wavefunctions was set at 450 eV for all structures and each structure was optimized until forces on single atoms were less than 0.01 eV/Å.

For the cluster structures, the binding energies between AQS (or DMSO) and PbI_2 were calculated as

$$E_{binding}(\text{DMSO-PbI}_2) = E(\text{total}) - E(\text{DMSO}) + E(\text{PbI}_2)$$

$$E_{binding}(\text{AQS-PbI}_2) = E(\text{total}) - E(\text{AQS}) + E(\text{PbI}_2)$$

where E (total) is the total energy of PbI_2 upon DMSO or AQS adsorption; E

(DSMO), *E* (AQS), and *E* (PbI_2) are the energies of isolated DMSO molecule, AQS molecule, and PbI_2 cluster, respectively.

For the crystal structures, the formation energies for DSMO-PbI_2 and AQS-DSMO-PbI_2 were calculated as

$$E_{formation}\ (\text{DSMO-PbI}_2) = E\ (\text{total}) - E\ (\text{DMSO}) - E\ (\text{PbI}_2)$$

$$E_{formation}\ (\text{AQS-DSMO-PbI}_2) = E\ (\text{total}) - E\ (\text{AQS}) - E\ (\text{DMSO}) - E\ (\text{PbI}_2)$$

where *E* (total) is the total energy for DSMO-PbI_2 or AQS-DSMO-PbI_2 crystal, and *E* (AQS), *E* (DMSO), and *E* (PbI_2) are the energies of AQS molecules, DMSO molecules, and PbI_2 crystal, respectively.

The geometries optimizations, electrostatic potential and dipole moment calculations of CF_3-PMA^+ ($FPMA^+$) and CF_3-PEA^+ ($FPEA^+$) molecules were performed at B3LYP/6-311G(d, p) level using Gaussian09 package[1].

Supporting Figures and Tables

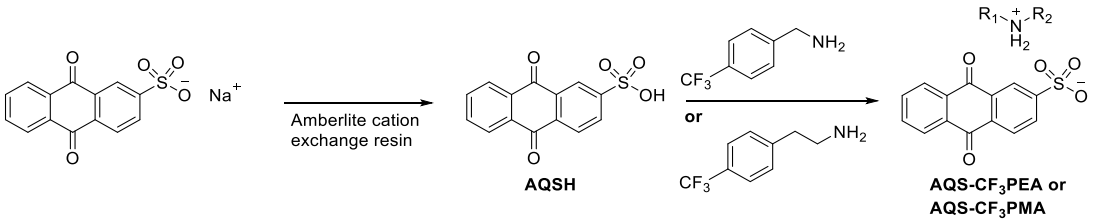

Scheme S1. The synthesis route of AQS-based additives.

Synthesis of **AQSH**: Sodium anthraquinone-2-sulfonate (300 mg, 0.97 mmol) and 3 mL Amberlite cation exchange resin (IR-120 hydrogen form) were added in 5 mL deionized water. The mixture was stirred overnight when the anthraquinone compound was dissolved. Then the solution was flushed over a cation exchange column with Amberlite cation exchange resin again. The obtained sulfonic acid was evaporated and the compound was dried under vacuum overnight. The product was obtained as pale-yellow powder with a yield of 216 mg (yield: 77%). ^{1}H NMR (400 MHz, D_2O) δ 8.07 (s, 1H), 7.97 (d, *J* = 8.2 Hz, 1H), 7.88 (d, *J* = 8.2 Hz, 1H), 7.74 – 7.64 (m, 2H), 7.58 – 7.50 (m, 2H). ^{13}C NMR (101 MHz, D_2O) δ 182.46, 182.36,

148.04, 135.15, 135.10, 133.38, 132.32, 131.57, 131.18, 127.81, 126.72, 123.74. (two peaks overlap).

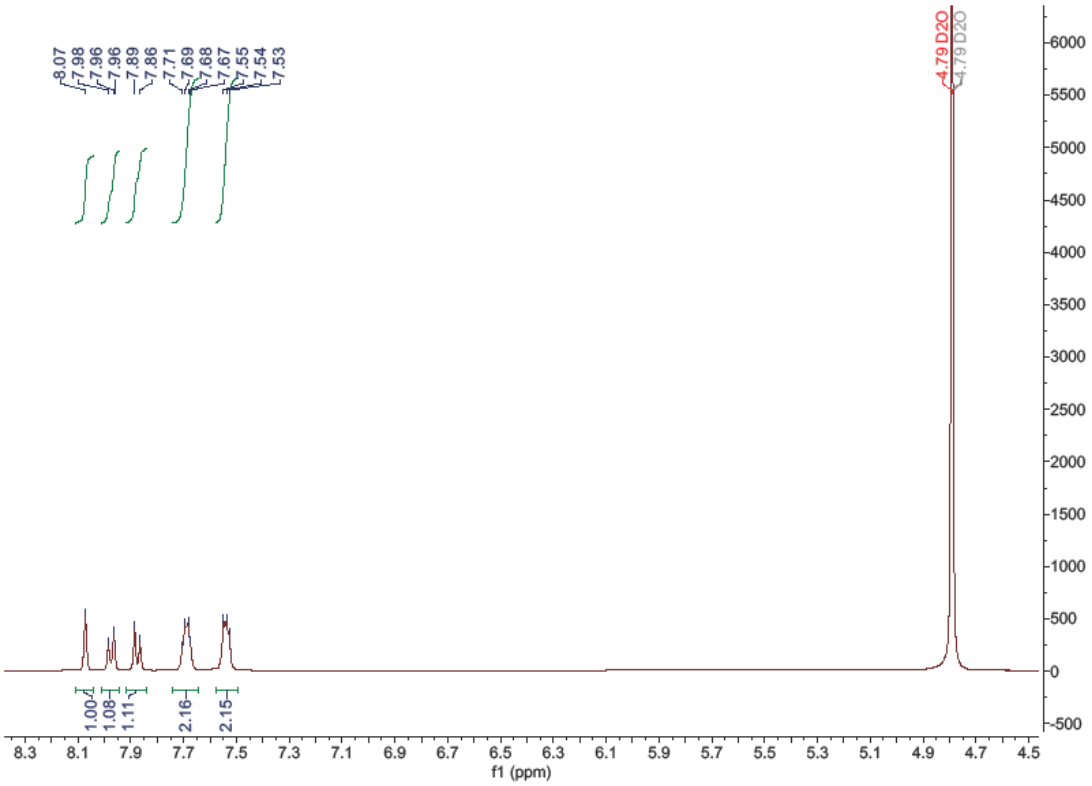

Figure S1. The ^{1}H NMR spectra of AQSH.

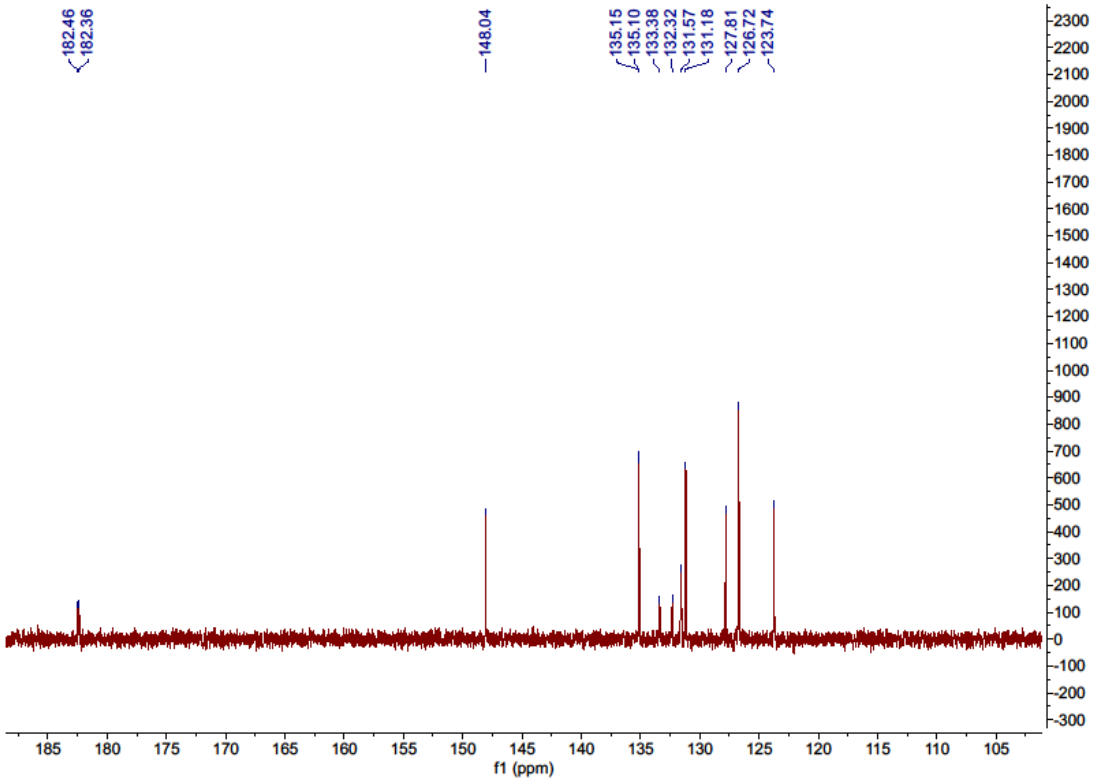

Figure S2. The ^{13}C NMR spectra of AQSH.

Synthesis of **AQS-CF$_3$PEA** (AQS:FPEA): The **AQSH** aqueous (0.97 mmol) solution obtained as mentioned above was cooled to 0 ℃ and then 2-(4-Trifluoromethylphenyl)ethylamine (1.1 mmol) was added to convert the acid to ammonium salt. The water was evaporated and the compound was dried under vacuum overnight. The product was obtained as light-yellow powder with a yield of 398 mg (yield: 86%). ^{1}H NMR (400 MHz, DMSO-d_6) δ 8.41 (s, 1H), 8.31 – 8.15 (m, 2H), 8.15 – 8.04 (m, 1H), 8.04 – 7.88 (m, 2H), 7.88 – 7.61 (m, 4H), 7.60 – 7.24 (m, 2H), 3.11 (t, J = 7.6 Hz, 2H), 2.96 (t, J = 7.6 Hz, 2H). ^{13}C NMR (101 MHz, DMSO) δ 182.36, 182.15, 153.50, 142.21, 134.62, 134.56, 133.19, 133.17, 132.96, 132.92, 131.24, 129.68, 127.71, 127.39, 127.11, 126.84, 125.71, 125.46, 125.42, 123.73, 32.81.

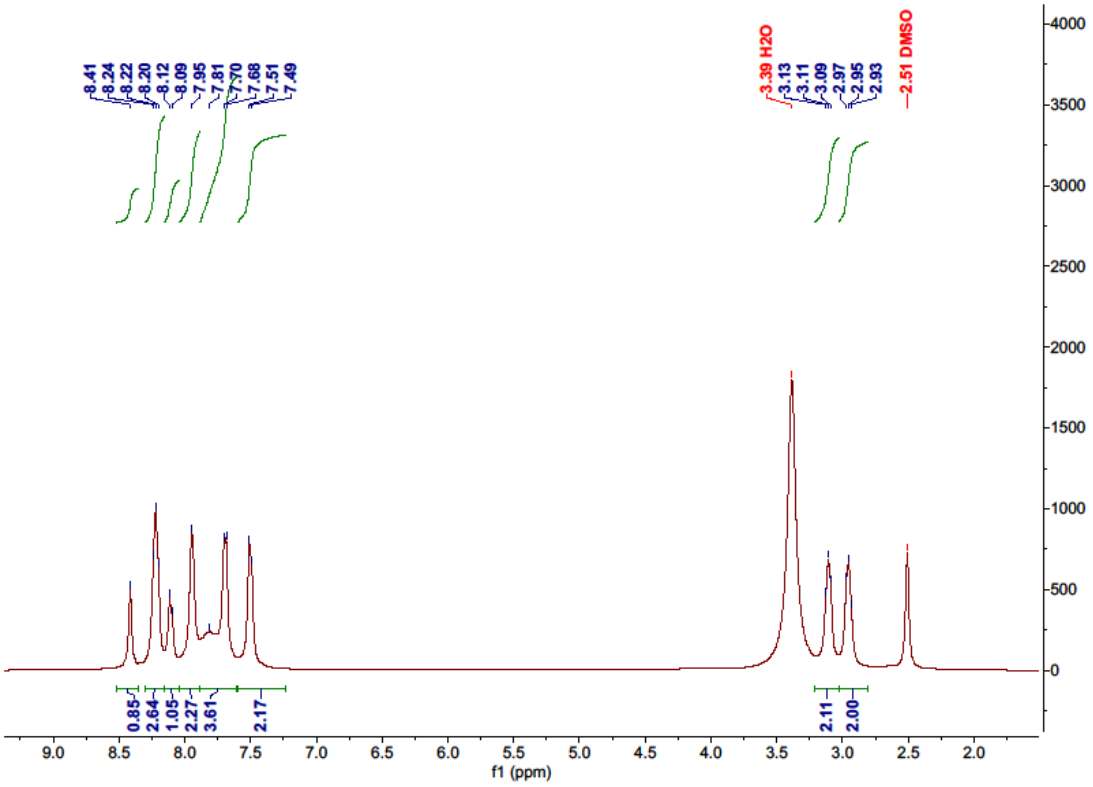

Figure S3. The ^{1}H NMR spectra of AQS-CF3PEA (AQS:FPEA).

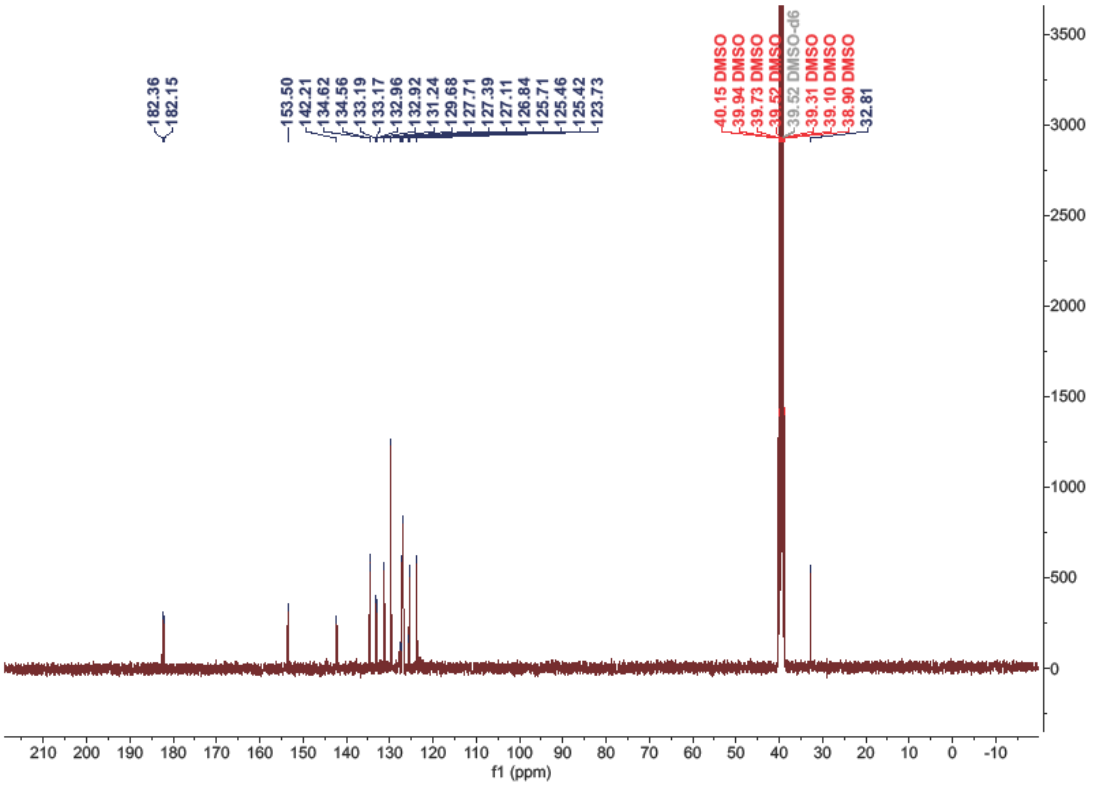

Figure S4. The ^{13}C NMR spectra of AQS:FPEA.

Synthesis of **AQS-CF$_3$PMA** (AQS:FPMA): The **AQSH** aqueous solution (0.97 mmol) obtained as mentioned above was cooled to 0 ℃ and then 1.2 equiv 4-(Trifluoromethyl)benzylamine was added to convert the acid to ammonium salt. The water was evaporated and the compound was dried under vacuum overnight. The product was obtained as light-yellow powder with a yield of 323 mg (yield: 72%). ^{1}H NMR (400 MHz, DMSO-d_6) δ 8.41 (s, 1H), 8.37 – 8.03 (m, 7H), 8.03 – 7.75 (m, 4H), 7.75 – 7.51 (m, 2H), 4.17 (s, 2H). ^{13}C NMR (101 MHz, DMSO) δ 182.35, 182.14, 153.51, 138.72, 134.61, 134.55, 133.19, 133.16, 132.94, 132.90, 131.22, 129.67, 129.15, 128.83, 127.08, 126.83, 125.53, 123.72, 122.77, 41.81

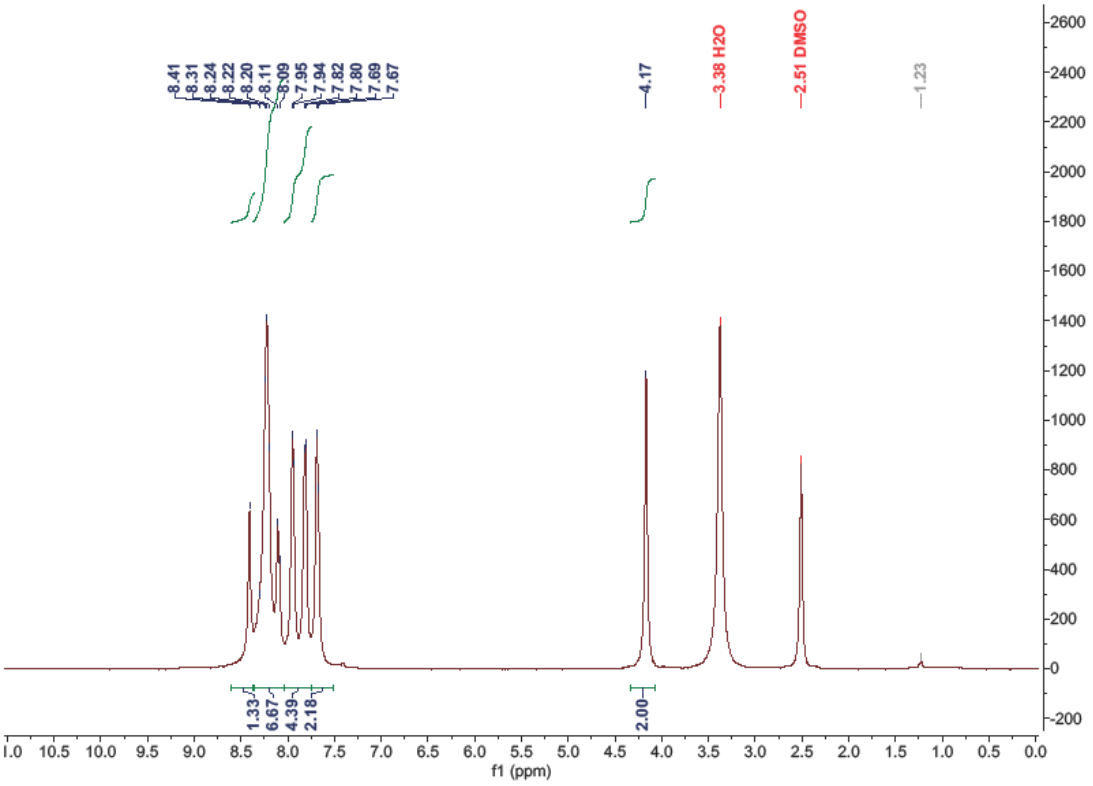

Figure S5. The ^{1}H NMR spectra of AQS:FPMA.

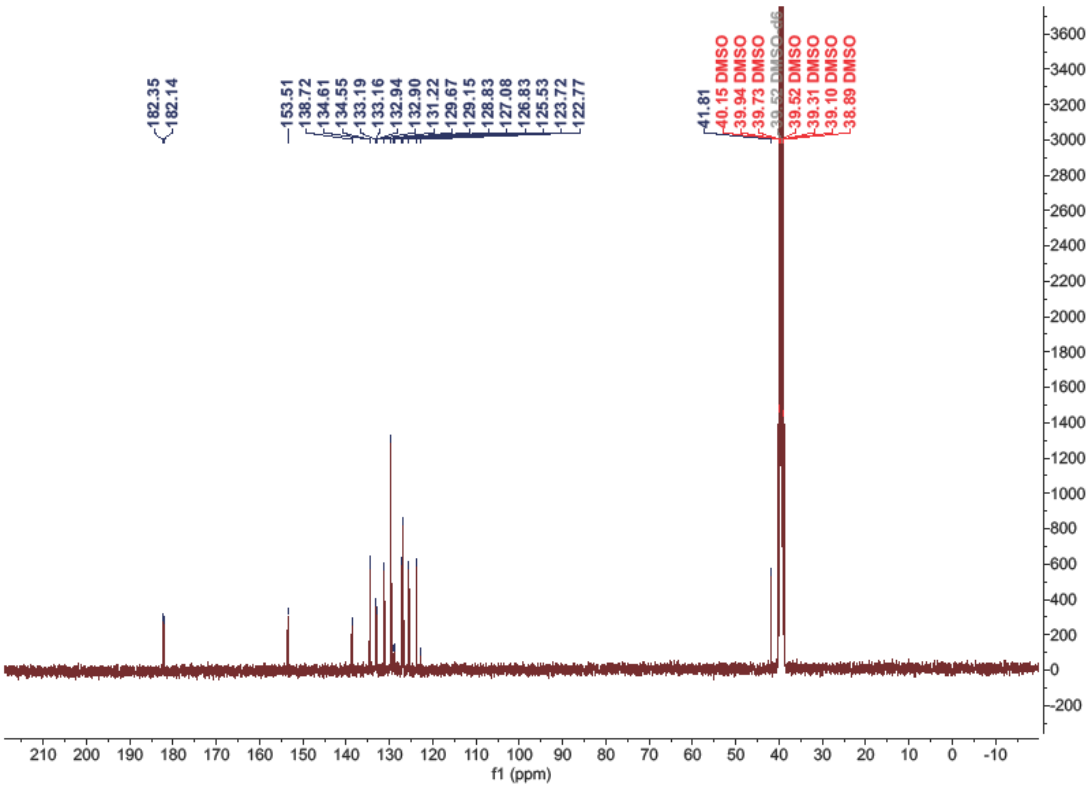

Figure S6. The ^{13}C NMR spectra of AQS:FPMA.

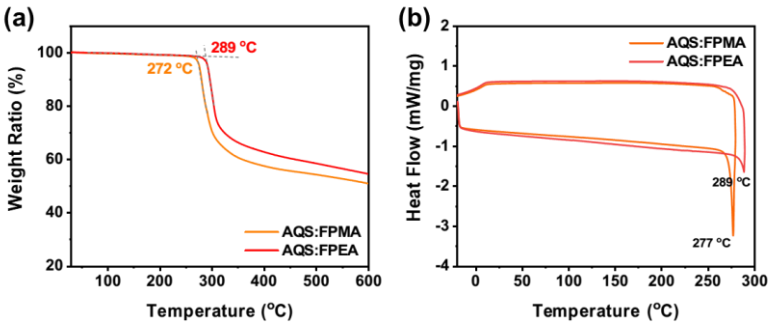

Figure S7. (a)TGA and (b) DSC thermograms of AQS:FPMA and AQS:FPEA.

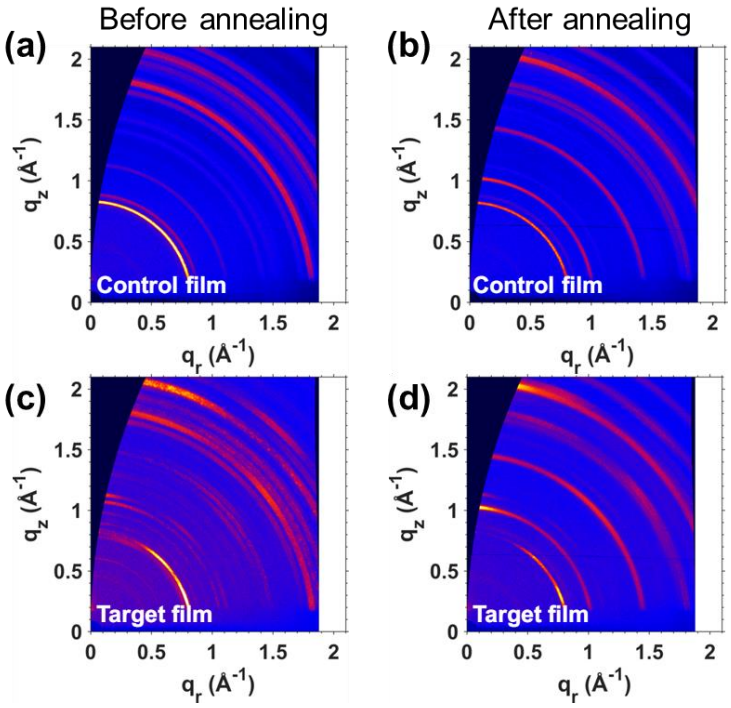

Figure S8. 2D-GIWAXS patterns of control film (a, b) and target film (c, d) before annealing and after annealing.

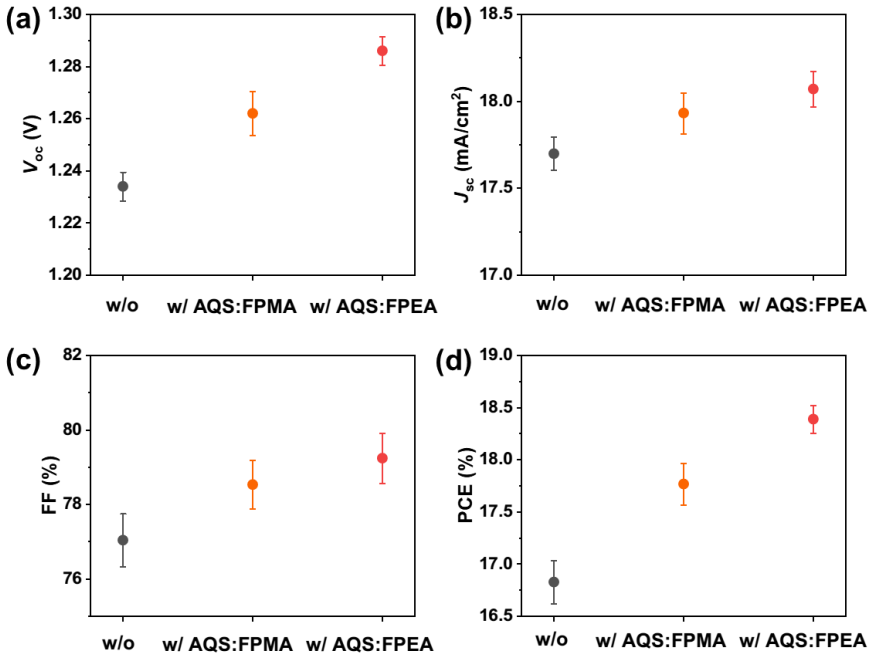

Figure S9. The statistics of (a) V_{oc}, (b) J_{sc}, (c) FF and (d) PCE corresponding to single-junction i-PSCs.

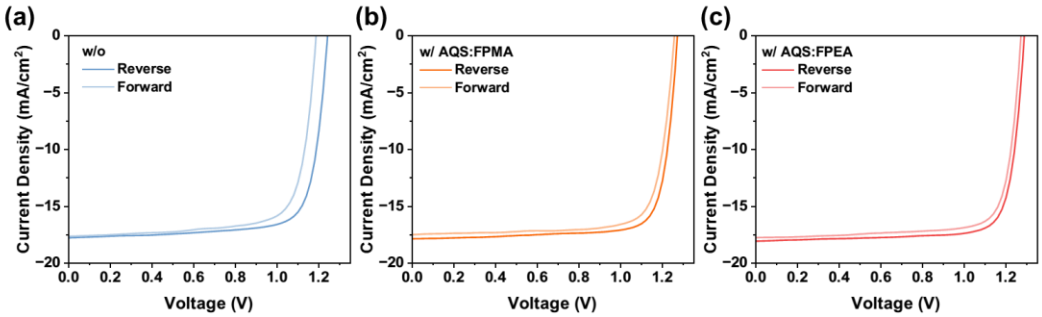

Figure S10. The *J-V* characteristics of devices with different additives in forward and reverse scan.

Table S1. The statistic of parameters of devices with different additives in forward and reverse scan.

Additive	Scan mode	V_{oc} (V)	J_{sc} (mA/cm^2)	FF (%)	PCE (%)
w/o	Reverse	1.24	17.80	77.18	17.04
	Forward	1.19	17.62	75.11	15.75
w/ AQS:FPMA	Reverse	1.27	17.83	79.38	17.97
	Forward	1.26	17.52	77.68	17.15
w/ AQS:FPEA	Reverse	1.29	18.07	79.74	18.59
	Forward	1.27	17.72	78.69	17.71

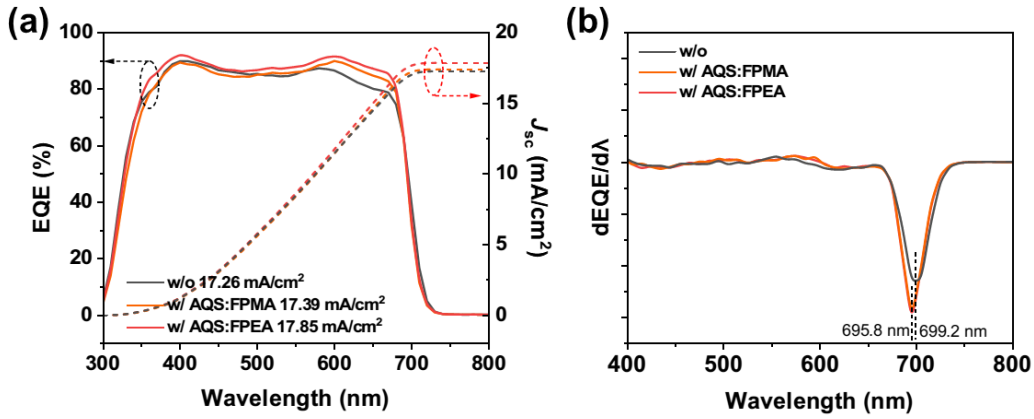

Figure S11. (a) EQE curves and (b) corresponding derivative curves of i-PSCs w/o additive, w/ AQS:FPMA and w/ AQS:FPEA.

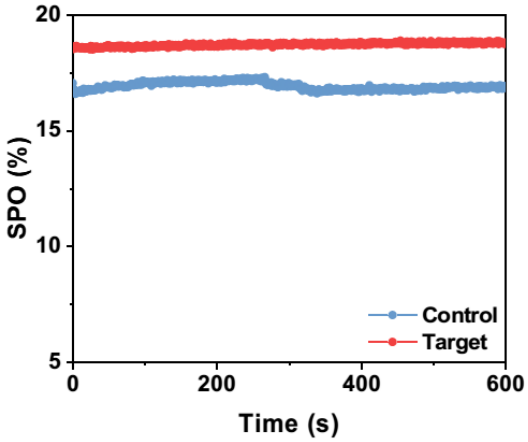

Figure S12. The stabilized power output (SPO) of single-junction i-PSCs.

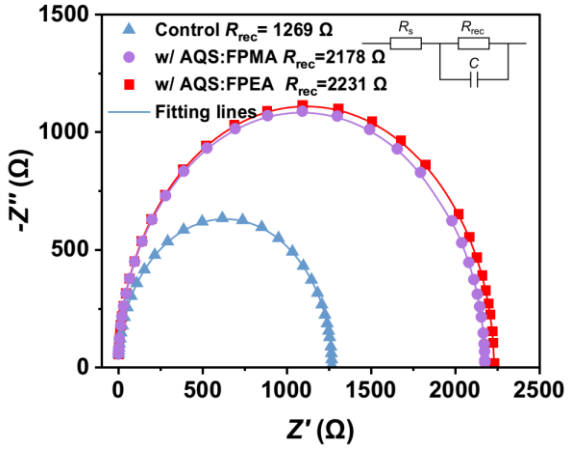

Figure S13. The Nyquist plots of electrochemical impedance spectroscopy performed on control, w/ AQS:FPMA, and w/ AQS:FPEA PSCs. The inset is the equivalent circuit model.

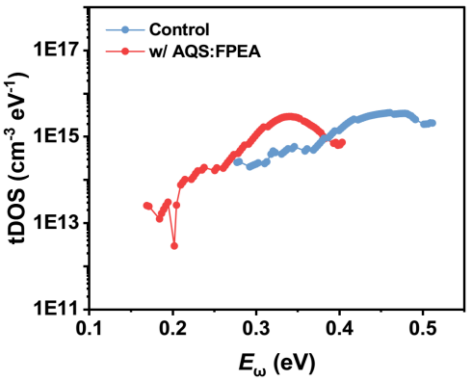

Figure S14. Trap density of states (tDOS) as function of E_ω under room temperature.

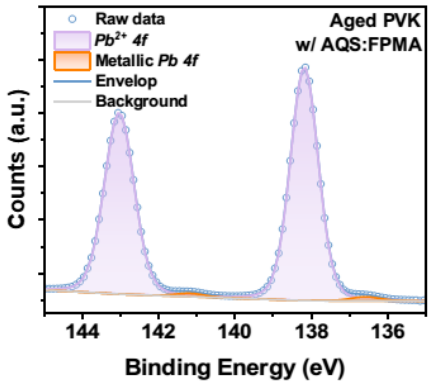

Figure S15. The *Pb 4f* high-resolution XPS spectra of the aged perovskite with AQS:FPMA.

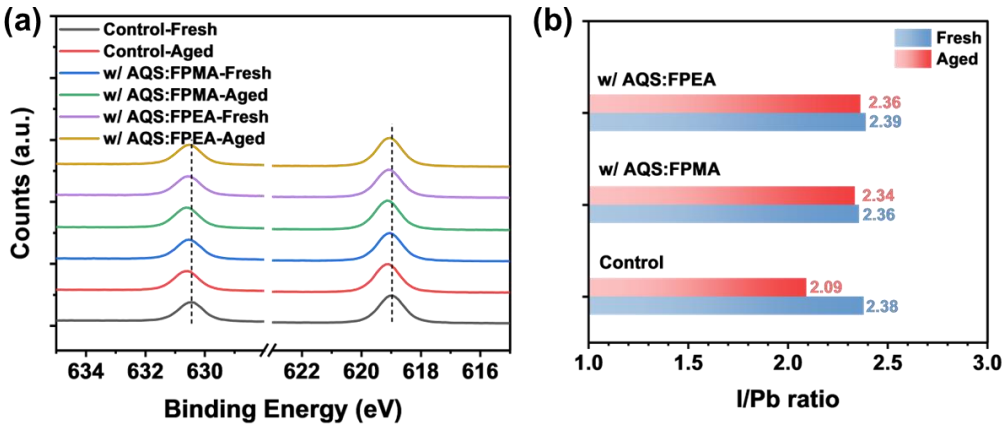

Figure S16. (a) The *I 3d* high-resolution XPS spectra of fresh and aged perovskite films. (b) The statistic of I/Pb ratio of fresh and aged perovskite films.

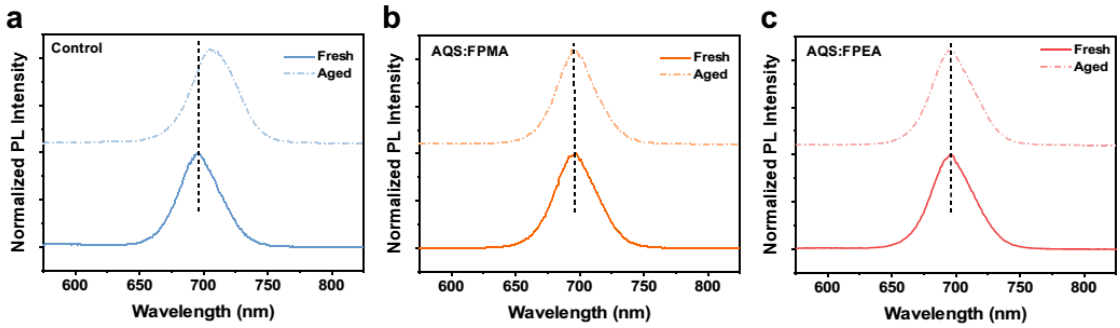

Figure S17. The PL spectra of the (a) control, (b) w/ AQS:FPMA and (c) w/ AQS:FPEA perovskite films. The aged films were obtained by exposing them under continuous laser irradiation for 10 minutes.

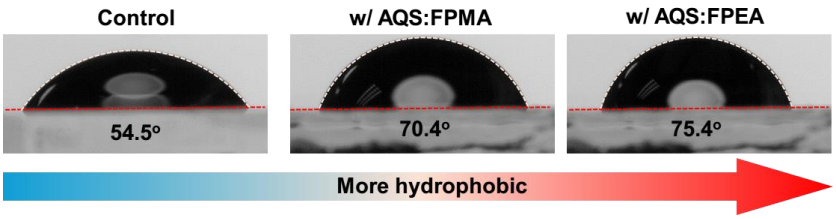

Figure S18. The contact angle photograph of water on different perovskite films.

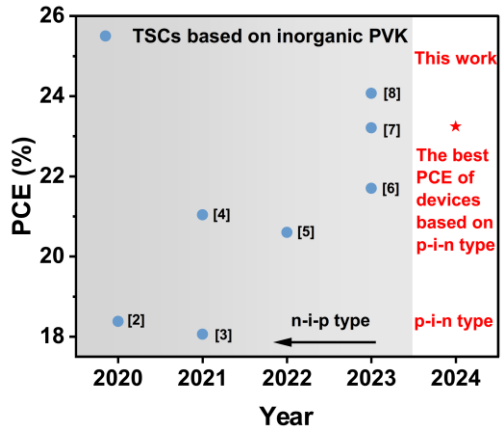

Figure S19. The statistics of P/dO TSCs based on inorganic perovskites.[2–8] This work achieves the best PCE among inverted P/O TSCs based on inorganic perovskites.

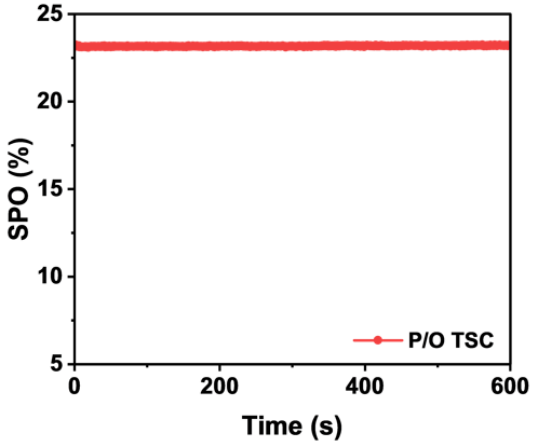

Figure S20. The stabilized power output (SPO) of the inverted P/O TSC.

Table S2. The parameter statistic of signle-junction OSC, PSC and P/O TSC.

Device	V_{oc} (V)	J_{sc} (mA/cm^2)	FF (%)	PCE (%)
OSC	0.86	27.22	76.30	17.86
PSC	1.29	18.07	79.74	18.59
P/O TSC	2.11	14.38	76.58	23.24

References

[1] M. J. Frisch, G. W. Trucks, H. B. Schlegel, G. E. Scuseria, M. A. Robb, J. R. Cheeseman, G. Scalmani, V. Barone, G. A. Petersson, H. Nakatsuji, X. Li, M. Caricato, A. V. Marenich, J. Bloino, B. G. Janesko, R. Gomperts, B. Mennucci, H. P. Hratchian, J. V. Ortiz, A. F. Izmaylov, J. L. Sonnenberg, D. Williams-Young, F. Ding, F. Lipparini, F. Egidi, J. Goings, B. Peng, A. Petrone, T. Henderson, D. Ranasinghe, V. G. Zakrzewski, J. Gao, N. Rega, G. Zheng, W. Liang, M. Hada, M. Ehara, K. Toyota, R. Fukuda, J. Hasegawa, M. Ishida, T. Nakajima, Y. Honda, O. Kitao, H. Nakai, T. Vreven, K. Throssell, J. A. Montgomery Jr., J. E. Peralta, F. Ogliaro, M. J. Bearpark, J. J. Heyd, E. N. Brothers, K. N. Kudin, V. N. Staroverov, T. A. Keith, R. Kobayashi, J. Normand, K. Raghavachari, A. P. Rendell, J. C. Burant, S. S. Iyengar, J. Tomasi, M. Cossi, J. M. Millam, M. Klene, C. Adamo, R. Cammi, J. W. Ochterski, R. L. Martin, K. Morokuma, O. Farkas, J. B. Foresman, D. J. Fox, **2009**.

[2] S. Xie, R. Xia, Z. Chen, J. Tian, L. Yan, M. Ren, Z. Li, G. Zhang, Q. Xue, H.-L. Yip, Y. Cao, *Nano Energy* **2020**, *78*, 105238.

[3] X. Wu, Y. Liu, F. Qi, F. Lin, H. Fu, K. Jiang, S. Wu, L. Bi, D. Wang, F. Xu, A. K.-Y. Jen, Z. Zhu, *J. Mater. Chem. A* **2021**, *9*, 19778–19787.

[4] W. Chen, D. Li, X. Chen, H. Chen, S. Liu, H. Yang, X. Li, Y. Shen, X. Ou, Y. (Michael) Yang, L. Jiang, Y. Li, Y. Li, *Adv. Funct. Mater.* **2022**, *32*, 2109321.

[5] X. Gu, X. Lai, Y. Zhang, T. Wang, W. L. Tan, C. R. McNeill, Q. Liu, P. Sonar, F. He, W. Li, C. Shan, A. K. K. Kyaw, *Advanced Science* **2022**, *9*, 2200445.

[6] X. Lai, S. Chen, X. Gu, H. Lai, Y. Wang, Y. Zhu, H. Wang, J. Qu, A. K. K. Kyaw, H. Xia, F. He, *Nat Commun* **2023**, *14*, 3571.

[7] S. Sun, X. Xu, Q. Sun, Q. Yao, Y. Cai, X. Li, Y. Xu, W. He, M. Zhu, X. Lv, F. R. Lin, A. K. -Y. Jen, T. Shi, H. Yip, M. Fung, Y. Xie, *Advanced Energy Materials* **2023**, *13*, 2204347.

[8] S. Jiang, R. Wang, M. Li, R. Yu, F. Wang, Z. Tan, *Energy Environ. Sci.* **2023**, 10.1039.D3EE02940A.d